Water Supply

Water Supply Vol 22 No 1, 391 doi: 10.2166/ws.2021.263

Quantitative assessment of the dynamics and attribution of arable land water scarcity for arid and semiarid areas based on water footprint framework: the Inner Mongolia case

Yuanyuan Wang[a,b], Fanhao Meng [a,b,*] and Min Luo[a,b]

[a] College of Geographical Science, Inner Mongolia Normal University, Hohhot 010022, China
[b] Inner Mongolia Key Laboratory of Remote Sensing and Geographic Information Systems, Inner Mongolia Normal University, Hohhot 010022, China
*Corresponding author. E-mail: mfh320@imnu.edu.cn

FM, 0000-0002-0450-0542

ABSTRACT

Growing water shortages have been a systemic risk around the world, especially in arid and semi arid areas, seriously threatening global food security and human well-being. Reasonable and accurate evaluations of the water shortages of cultivated lands provide scientific reference for irrigation strategies. In this study, to better understand the distribution and cause of water scarcity for arid and semiarid areas, we used the arable land water scarcity index (AWSI), based on water footprint theory, to accurately estimate the temporal and spatial patterns of the AWSI of Inner Mongolia in China over 1999–2018, and further reveal the key factors influencing the AWSI distribution. The AWSI distribution pattern of Inner Mongolia was high in the southwest and low in the northeast, with an average value of 0.63 and indicating high water stress for a long time. The AWSI presented an increasing trend in 1999–2018, being slow in the west (change rate$<$2%) and fast in the east ($\geq$2%). The main factors that significantly affected the AWSI were precipitation, relative humidity, and agricultural planting area. This study can provide scientific reference for the formulation of agricultural water management and sustainable use strategies in arid and semiarid areas.

Key words: arable land water scarcity index, arid and semiarid areas, Inner Mongolia, water footprint, water stress

HIGHLIGHTS

- In addition to green and blue water, grey water is also taken into account in AWSI assessment.
- The spatiotemporal distribution of AWSI in arid and semi arid areas is accurately evaluated.
- The spatiotemporal heterogeneity between AWSI, AWR and CWF in arid and semi arid areas is revealed.
- Precipitation and agricultural planting area are the main controlling factors of water shortage distribution pattern in arid and semi arid areas.

GRAPHICAL ABSTRACT

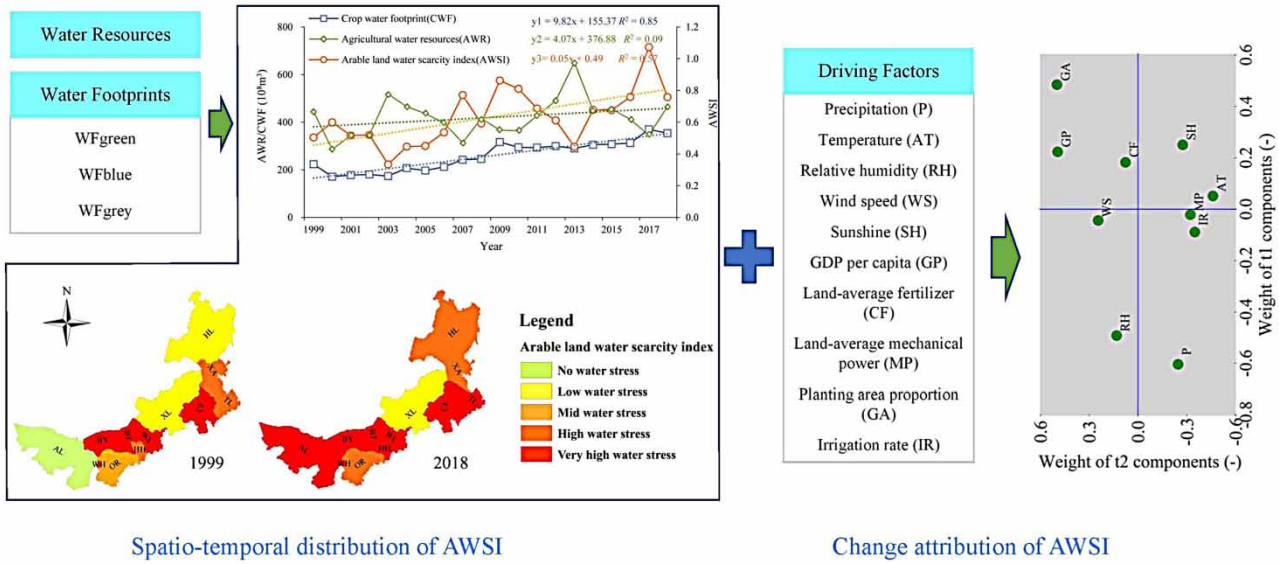

1. INTRODUCTION

The combined areas of global arid and semiarid regions account for approximately 40% of total land area and have always faced water shortage (Huang *et al.* 2016). The northern and central parts of the United States, the Russian Far East, and the northern and north eastern regions of China have all suffered severe water shortage in the past half-century (Zhai *et al.* 2017; Zhao *et al.* 2020; Zhou *et al.* 2020). Agriculture is the sector most vulnerable to water conditions (Dai *et al.* 2020) and water deficiency can result in severe consequences associated with grain yield reduction (Qader *et al.* 2018; Melandri *et al.* 2019). In the past 50 years, droughts affecting global crop production have reduced grain production by 9%–10%; thus, the scarcity of water resources poses major threats to regional food security and sustainable economic development (Lesk *et al.* 2016).

With increase in population, food consumption continues to increase. From 2010 to 2030, global agricultural land is expected to increase by 14% (Schneider *et al.* 2010). The human–land conflict in arid and semiarid areas is so prominent that ensuring food security has become a major issue in these countries. Inner Mongolia, a typical arid and semiarid region that includes the Hetao Plain and the Northeast Plain, is one of China's major grain-producing regions. Agricultural water use in Inner Mongolia continues to increase with the expansion of agricultural production, but the precipitation conditions in the region are very unsatisfactory (Wang *et al.* 2018; Song *et al.* 2020). Meanwhile, due to the lack of water and low soil organic matter content, serious degradation of arable land has brought great challenges to agricultural development. The excessive application of fertilizer to ensure crop yields has caused a series of environmental problems, such as source pollution, soil degradation and desertification (Li *et al.* 2018). Land degradation and desertification may further lead to serious sandstorms (Huang *et al.* 2020), which directly threaten the sustainable development of human society. Those studying the sustainable development of water resources list water shortage assessments as the main research object. Over time, the method for determining water shortages has expanded and improved, but the quantitative assessment of the water shortage status of arable land in Inner Mongolia is insufficient due to problems such as an inadequate understanding of the causes of change. Comprehensive and accurate assessments of water shortages, especially in arid and semi arid areas, provide a scientific basis through which strategies for coping with climate change, the sustainable development and utilization of water resources, and food security can be proposed (Gosling & Arnell 2016; Tripathi *et al.* 2016).

At present, several indicators have been established to reflect the shortage of water resources in regions with arable land. Fox example, considering the important role of irrigation water, Falkenmark *et al.* (1989) published the water pressure index (WPI). The WPI takes the amount of water resources per capita as a standard to measure the scarcity of water resources in an area. When the amount of water resources per capita is less than 1,700 $m^3 \cdot a^{-1}$, the region begins to face the pressure of water resources; when the amount is less than 1,000 $m^3 \cdot a^{-1}$, the region faces a chronic water shortage. Raskin *et al.* (1997) used

direct water to replace the total water demand, accounting for the relationship between direct water and available water resources, to develop the water resource vulnerability index (WRVI). For this index, the standard of water shortage is $20\% \leq \text{WRVI} \leq 40\%$, and when $\text{WRVI} > 40\%$, it is defined as a severe water shortage. Liu *et al.* (2017) calculated the ratios of blue water and grey water to the water resources in a basin to determine the water shortage using a series of water shortage assessment methods. However, the above indexes do not include green water in the evaluation of water resource shortages. Natural precipitation (i.e. green water) used by crops is also important because it can replace irrigation water, thereby alleviating the pressure on water resources (Egan 2011). Comprehensive consideration of regional blue water, green water and grey water footprints is the core of water footprint theory (Castellanos *et al.* 2016). Since the theory considers the direct and indirect water consumption of all processes in the production of an agricultural product, it has been widely used by scholars since its introduction in 2002 (Xinchun *et al.* 2017a, 2017b; Qian *et al.* 2018; Xu *et al.* 2019; Zhang *et al.* 2019). In agricultural production, the loss of the surface water and groundwater from irrigation water is considered the blue water footprint. The green water footprint comprises rainwater that does not form runoff or recharge groundwater after precipitation, but remains in the soil and can be used by plants through evapotranspiration. Water resources that have experienced pollution from fertilizers and pesticides are defined as grey water. After the grey water footprint is calculated, the problem of quantitatively explaining the pollution of arable land water can be solved (Zhao *et al.* 2019). Xinchun *et al.* (2017b) took into consideration the green water footprint and established the arable land water scarcity index (AWSI), based on the water footprint and generalized water resources, as a carrier to achieve the unification of generalized water resources and actual water consumption. Although the AWSI is expected to be evaluated in some areas, its applicability in arid and semi arid regions is unclear.

This study focuses on water footprint theory and, taking Inner Mongolia as the research area, uses CROPWAT 8.0 software based on meteorological data, socioeconomic data, and water resource data to obtain the crop water footprint (including the green, blue and grey water footprints) and combine generalized water resources to establish the AWSI. To evaluate the current status of agricultural water resource revenue and expenditure in Inner Mongolia, we further analyse the spatial and temporal distributions of the AWSI through spatial autocorrelation and partial least squares regression to quantize the key factors influencing the water scarcity. This study's results can provide a scientific reference for the formulation of reasonable and sustainable agricultural water use programmes of relevant government departments.

2. MATERIALS AND METHODS

2.1. Study area

Inner Mongolia Autonomous Region (Inner Mongolia, 37°24′–53°23′N, 97°12′–126°04′E) is a typical arid and semiarid area located in northern China, covering an area of 1.18×10^6 km^2, ranging from 85 to 3,526 m of elevation, and containing 12 cities: Hohhot (HH), Baotou (BT), Hulunbuir (HL), Xing'an (XA), Tongliao (TL), Chifeng (CF), Xilingol (XL), Wulanchabu (WL), Ordos (OR), Bayannur (BY), Wuhai (WH) and Alashan (AL) (Figure 1). Inner Mongolia belongs to a typical temperate continental climate zone. The annual mean air temperature progressively increases from the northeast to the southwest, with temperature values of −4.5 °C to 9.8 °C, while the annual precipitation decreases from the northeast to the southwest, with 1,850 mm of annual potential evapotranspiration and approximately 2,900 h of total annual sunshine duration. Because of the distributions of rainfall and temperature, the land use types mainly include forests in HL; grassland in XL and OR; desert in AL and BY; and farmland in HL, XA, TL and CF.

According to the *2019 Statistical Yearbook*, the area of arable land in 2018 was 9.27×10^6 ha, and the planted areas of wheat, corn, beans and tubers were 0.67×10^6 ha, 3.72×10^6 ha, 1.17×10^6 ha and 0.43×10^6 ha, respectively. The four cities with the largest arable areas are HL, XA, CF and TL, which together account for 64% of the total arable land area of the region. The total amount of water resources in Inner Mongolia is more than 461.53×10^8 m^3, and the four cities listed above account for 76% of the total. The total water consumption is 192.09×10^8 m^3, of which the national economic water consumption is 167.04×10^8 m^3; primary industry uses 139.89×10^8 m^3; of water, of which farmland irrigation uses 124.15×10^8 m^3; this shows that agricultural water accounts for 88.57%, 74.25%, and 64.58% of the water used in primary industry, the national economy, and total water consumption, respectively. Thus, agricultural water is the main water sector in the region.

2.2. Dataset

The observation data used in this study covered the period of 1999–2018 (20 years). The data used in this study mainly include: (1) meteorological data, for which monthly data from 46 meteorological stations in Inner Mongolia over the past

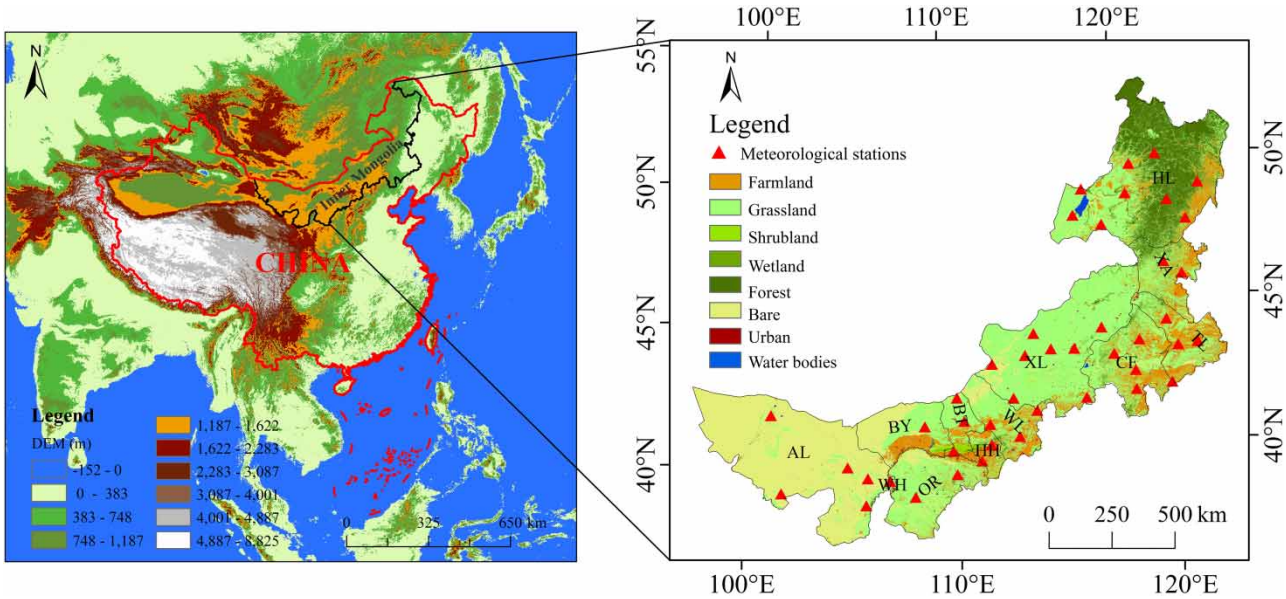

Figure 1 | Land use cover and locations of meteorological stations in Inner Mongolia (source of land use cover data: http://www.globeland30.org).

20 years, including information such as the monthly average maximum temperature, monthly average minimum temperature, monthly total precipitation, average wind speed, number of sunshine hours and relative humidity, were collected from the National Meteorological Centre (http://www.nmic.cn/); (2) statistical data, including information regarding the arable land area, crop planting area and yield, fertilizer application rate, total mechanical power, effective irrigation area and per capita GDP of the 12 cities in Inner Mongolia, which were acquired from the *Inner Mongolia Statistical Yearbook*; (3) agricultural production data, including the crop growth period data, which were mainly obtained from the temporal agricultural data of the Ministry of Agriculture and Rural Affairs of the People's Republic of China (http://www.moa.gov.cn/) and the crops database of the FAO (http://www.fao.org/); (4) water resource data, including the total water resources, total water consumption and agricultural water consumption, which were downloaded from the *Inner Mongolia Autonomous Region Water Resources Bulletin*.

2.3. Methods

2.3.1. Arable land water scarcity index

The arable land water scarcity index (AWSI), based on the water footprint and generalized water resources, aims to achieve an organic combination of generalized water resources and actual water consumption while comprehensively reflecting the internal relationship between regional agricultural water demand and actual water supply to efficiently assess the scarcity of arable land water resources and formulate water resource management strategies (Xinchun *et al.* 2017b). The AWSI is affected by factors such as climatic conditions, the proportion of arable land, the degree of irrigation and the mechanical level and is expressed as the ratio of the total crop water footprint of the region to the generalized water resources of that region:

$$AWSI = CWF/AWR \tag{1}$$

where $AWSI$ is the arable land water scarcity index, dimensionless; CWF is the total water footprint of regional crops, m^3; and AWR denotes the generalized water resources of regional agriculture, m^3.

$$AWR = AWR_b + AWR_g \tag{2}$$

where AWR_b is the amount of blue water resources that the region can provide, m^3; and AWR_g is the amount of green water resources that the region can provide, m^3.

$$AWR_b = TWR \times (AWU/TWU) \tag{3}$$

where TWR is the total amount of regional water resources, m^3; TWU is the total water consumption, m^3; and AWU is the agricultural water consumption, m^3.

$$AWR_g = 10 \times A \times P_{eff} \tag{4}$$

$$P_{eff} = \begin{cases} [P(4.17 - 0.02 \times P)]/4.17 & P \le 83 \text{ mm} \\ 4.17 + 0.1 \times P & P > 83 \text{ mm} \end{cases} \tag{5}$$

where A is the area of arable land, ha; and P and P_{eff} are monthly precipitation and monthly effective precipitation, respectively, mm.

A high AWSI indicates that the region is facing great pressure on water resources. The AWSI classification and the corresponding water stress levels are shown in Table 1.

2.3.2. Crop water footprint

The CROPWAT 8.0 software was developed by the United Nations Food and Agriculture Organization (FAO) (Raphael *et al.* 2018). The software can calculate crop water demand and irrigation based on existing or new climate and crop data. In addition, irrigation plans can be formulated for different management conditions, and planned water supply can be calculated for different crop modes.

The reference crop evapotranspiration ET_0 is calculated, and the concept of ET_0 is introduced to study the atmospheric evaporation requirements that are not related to crop types, crop development or crop management practices. Therefore, the only factors that affect ET_0 are climatic parameters. The CROPWAT model uses the Penman–Monteith formula (Singh Rawat *et al.* 2019) to calculate the reference crop evapotranspiration based on the monthly average minimum temperature, maximum temperature, relative humidity, wind speed, sunshine hours and other weather data in the study area:

$$ET_0 = \frac{0.408\Delta(R_n - G) + \gamma 900/(T_a + 273)u_2(e_s - e_a)}{\Delta + \gamma(1 + 0.34u_2)} \tag{6}$$

where ET_0 is the reference crop evapotranspiration, $mm \cdot d^{-1}$; Δ is the slope of the saturated water pressure and temperature curve, $kPa \cdot °C^{-1}$; R_n is the net radiation of the reference crop canopy surface, $MJ \cdot (m^2 \cdot d)^{-1}$; G is the soil heat flux, $MJ \cdot (m^2 \cdot d)^{-1}$; γ is the dry–wet surface constant, $kPa \cdot °C^{-1}$; T_a is the daily average air temperature at a height of 2 m, °C; u_2 is the wind speed at a height of 2 m, $m \cdot s^{-1}$; e_s is the saturated water vapor pressure, kPa; and e_a is the actual water vapor pressure, kPa.

To calculate crop evapotranspiration ET_C, the model refers to crop evapotranspiration and crop coefficients at different stages:

$$ET_C = K_C \times ET_0 \tag{7}$$

where ET_C is the crop evapotranspiration, mm; and K_C is the crop coefficient, according to the FAO's K_C database.

Table 1 | Category of water stress of farmland based on the arable land water scarcity index (AWSI)

AWSI	Water stress level
AWSI < 0.10	No water stress
0.10 ≤ AWSI < 0.20	Low water stress
0.20 ≤ AWSI < 0.40	Moderate water stress
0.40 ≤ AWSI < 0.80	High water stress
AWSI > 0.80	Very high water stress

Next, the blue, green and grey water footprints of the four main crops are calculated. The formula for calculating the regional green water footprint of a given crop is:

$$WF_{\text{green}} = CWR_{\text{green}} \times A \tag{8}$$

$$CWR_{\text{green}} = 10 \times \sum_{d=1}^{\lg p} ET_{\text{green}} \tag{9}$$

$$ET_{\text{green}} = min(ET_{\text{C}}, P_{\text{eff}}) \tag{10}$$

where WF_{green} represents the green water footprint of the crop, m^3; CWR_{green} is the green water usage of the crop, $m^3 \cdot ha^{-1}$; A is the planting area of the crop, ha; ET_{green} is the green water demand of the crop, mm; 10 is a constant conversion factor that converts the accumulated amount of water depth (mm) to the amount of water per unit land area, $m^3 \cdot ha^{-1}$; and the sum $\sum$ counts the accumulated number of days ($\lg p$–length of growth) of the process starting from the planting date and ending at the harvest date, indicating the length of the growth phase.

The formula for calculating the regional blue water footprint of a given crop is:

$$WF_{\text{blue}} = CWR_{\text{blue}} \times A \tag{11}$$

$$CWR_{\text{blue}} = 10 \times \sum_{d=1}^{\lg p} ET_{\text{blue}} \tag{12}$$

$$ET_{\text{blue}} = max(ET_{\text{C}} - P_{\text{eff}}, 0) \tag{13}$$

where WF_{blue} represents the blue water footprint of the crop, m^3; CWR_{blue} is the blue water consumption of the crop, $m^3 \cdot ha^{-1}$; and ET_{blue} is the blue water demand of the crop, mm.

The formula for calculating the regional grey water footprint of a given crop is:

$$WF_{\text{grey}} = (\alpha \times F)/(C_{\max} - C_{\text{nat}}) \tag{14}$$

where WF_{grey} is the grey water footprint of the crop, m^3; F is the amount of fertilizer application to the four main crops, kg; α is the amount of nitrogen leaching (that is, the proportion of pollution entering the water body, accounting for the total amount of nitrogen fertilizer application; this article selects 10% of nitrogen fertilizer application); $C_{\max}$ is the maximum allowable concentration of nitrogen fertilizer, which is set to 0.01 ($kg \cdot m^{-3}$) according to the Class III water standard of the *Surface Water Environmental Quality Standards* (GB3838–2002); and C_{nat} is the natural background concentration of pollutants, usually set to 0.

The regional crop production water footprint (CWF) refers to the amount of water resources consumed by crops during the growth process and is the sum of the blue, green, and grey water footprints of the main crops in the region:

$$CWF = WF_{\text{green}} + WF_{\text{blue}} + WF_{\text{grey}} \tag{15}$$

where CWF is the regional crop production water footprint, m^3.

2.3.3. Global spatial autocorrelation

The global spatial autocorrelation Moran's I can characterize the degree of correlation of a factor in a region to indicate the spatial distribution pattern of that factor. This study chooses Moran's I to illustrate the spatial distribution of the AWSI among the cities in Inner Mongolia. ArcGIS 10.7 software was used to calculate the global Moran's I specifically, and the closeness of neighbouring factors was quantified to show the overall spatial distribution of the AWSI. Assuming that this factor is randomly distributed in space, given the significance level $P \leq 0.1$ (i.e. Z-score ≥ 1.65), if $0 <$ Moran's $I < 1$, then there is a positive correlation, and the AWSI represents the aggregation characteristics in space; if $-1 <$ Moran's $I < 0$, there is a negative correlation. The closer Moran's I is to -1, the more scattered the AWSI is in each area and its surrounding area. If Moran's I is near 0, the original hypothesis cannot be rejected, and the AWSI is randomly distributed in space. The formula

is as follows:

$$I = \frac{n \sum_{i=1}^{n} \sum_{j=1}^{n} w_{i,j} z_i z_j}{S_0 \sum_{i=1}^{n} z_i^2} \tag{16}$$

$$S_0 = \sum_{i=1}^{n} \sum_{j=1}^{n} w_{i,j} \tag{17}$$

where I is Moran's I of spatial autocorrelation; n is the sum of the elements; S_0 is the aggregation of all spatial weights; z_i is the deviation of the attribute of element i from its average value; z_j is the deviation of the attribute of element j from its average value; and $w_{i,j}$ indicates the spatial weight between elements i and j.

2.3.4. Partial least-squares regression

Partial least-squares regression (PLSR) was used to analyse the factors influencing AWSI in this study. PLSR selects the latent factors that best explain the dependent variable from multiple variables, and the extracted latent factors also cover most of the information of the independent variable; this can remove duplicate relevant information and overcome multiple variables in the same regression of the equation. The cumulative importance index of parameters was also investigated (variable importance for the projection, VIP); the greater the VIP value, the greater the contribution of a potential factor. The weight of PLSR quantitatively describes the independent variables and various potential factors. Regression coefficients (RCs) are used to show the relationships between the propensity and size of the AWSI in PLSR and the independent variables. Proceed as follows:

(1) Find the eigenvector w_1, which corresponds to the largest eigenvalue of the matrix $E_0^T F_0 F_0^T E_0$, and find the component score vector $\hat{t}_1 = E_0 w_1$ and the residual matrix $E_1 = E_0 - \hat{t}_1 a_1^T$, where $a_1 = E_0^T \hat{t}_1 / ||\hat{t}_1||^2$.

where E_0 is the standardized $m \times n$ independent variable matrix; F_0 is the standardized $p \times n$ dependent variable matrix; E_0^T is the transposed matrix of E_0; F_0^T is the transposed matrix of F_0; and a_1 is the variable parameter in the regression model.

(2) Find the eigenvector w_2, which corresponds to the largest eigenvalue of the matrix $E_1^T F_0 F_0^T E_1$, and find the component score vector $\hat{t}_2 = E_1 w_2$ and the residual matrix $E_2 = E_1 - \hat{t}_2 a_2^T$, where $a_2 = E_1^T \hat{t}_2 / ||\hat{t}_2||^2$.

⋮

(r) To step r, find the eigenvector w_r, which corresponds to the largest eigenvalue of the matrix $E_{r-1}^T F_0 F_0^T E_{r-1}$, and obtain the component score vector $\hat{t}_r = E_{r-1} w_r$. The term r is the rank of E_0.

According to the cross-validity, it is determined that a total of $t_1 \ldots t_r$, r components are extracted. A satisfactory prediction model can be obtained, and the ordinary least squares regression equation is $F_0 = \hat{t}_1 \beta_1^T + \ldots + \hat{t}_r \beta_r^T + F_r$ on $\hat{t}_1 \ldots \hat{t}_r$ of F_0. The term β^T is obtained as the transposition of the parameter variables of the regression model.

Take $t_k = w_{k1}^* x_1 + \ldots + w_{km}^* x_m$ $(k = 1, 2, \ldots, r)$ into $\gamma = t_1 \beta_1 + \ldots + t_r \beta_r$, that is, the partial least squares regression equation of p dependent variables: $y_j = a_{j1} x_j + \ldots + a_{jm} x_m$ $(j = 1, 2, \ldots, p)$, where $w_k^* = (w_{k1}^*, \ldots, w_{km}^*)^T$ meet here $\hat{t}_k = E_0 w_k^*$, $w_k^* = \prod_{j=1}^{k-1} (I - w_j a_j^T) w_k$.

3. RESULTS AND DISCUSSION

3.1. AWR

The total annual average generalized agricultural water resources (AWR) of Inner Mongolia were calculated to be approximately $444.92 \times 10^8\ m^3$ with an upward trend during 1999–2018. The total AWR was determined jointly by the available green water (AWR_g) and blue water (AWR_b) resources, which were $139 \times 10^8\ m^3$ and $281 \times 10^8\ m^3$ respectively. The AWR and its composition in Inner Mongolia during the study period are shown in Figure 2.

As detailed in Figure 2, the AWR_g climbed slowly and varied between $83 \times 10^8\ m^3$ and $218 \times 10^8\ m^3$ in 2001 and 2018, yet the AWR_b maintained at a stable value, changing from 184×10^8 (in 2017) to 463×10^8 (in 2013), which means that

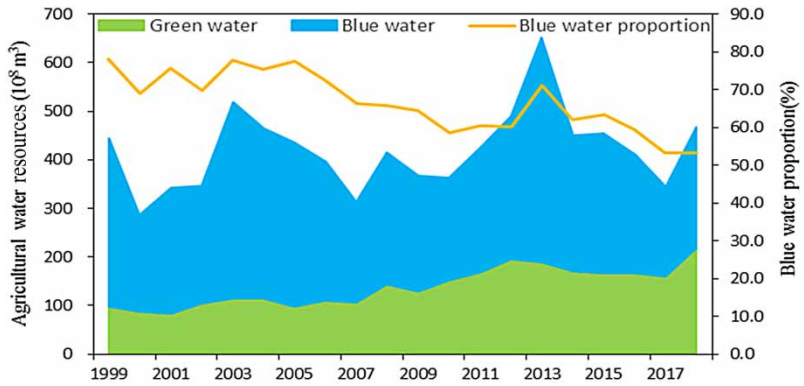

Figure 2 | Generalized agricultural water resources during 1999–2018 in Inner Mongolia, China.

inter-annual variation in the AWR_g was smaller than in the AWR_b. The AWR_g is jointly determined by precipitation and plenty of arable land. From 1999 to 2018, the area of farmland in Inner Mongolia showed an upward trend and went from 60.75×10^6 ha to 88.24×10^6 ha. Moreover, the ratio of precipitation in 2018 jumped by 65% compared with 1999. Therefore, AWR_g rose over time. The AWR_b was determined by the agricultural water usage (AWU) and water supply structure. Neither the total water resources (TWR) nor the total water usage (TWU) showed noticeable changes during the study period at 444.92×10^8 m^3 and 179.69×10^8 m^3, respectively. Although the AWU changed from 152.84×10^8 m^3 in 1999 to 140.84×10^8 m^3 in 2018, its variation was not significant. Thus, the water use structure remained stable, which directly caused a period of stability of AWR_b, yielding the rise and fall in AWR_b. Figure 2 also reveals that the AWR_b was a major component of agricultural water resources, and accounted for 66.7% of the AWR during 1999–2018, and moreover, this rate sank from 78% to 53% with the change of AWR_g.

The amount of AWR in typical years in 12 cities and the proportion of the AWR in each city to the total water resources in 1999–2018 are displayed in Figure 3. Spatially, the AWR was high in the cities located in the northeast but low in the southwest. The cities with similar AWR values presented significant aggregation.

The AWR was below 10×10^8 m^3 in WH and AL, all of which are in the southwest of Inner Mongolia. The AWR of WH was only 0.18×10^8 m^3, which ranked the lowest in Inner Mongolia. They are far from the sea and blocked by mountains, resulting in

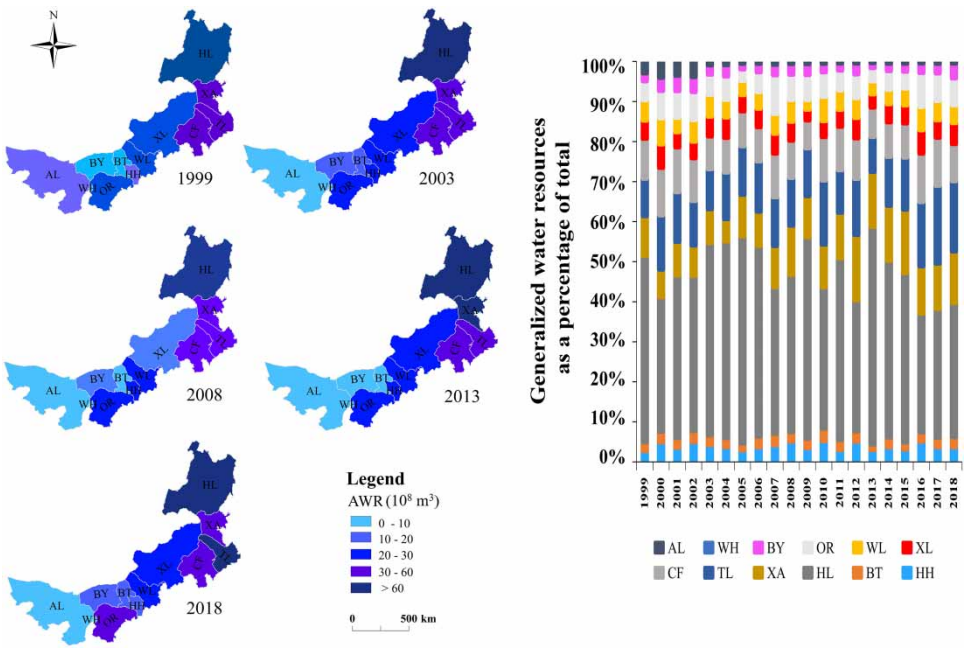

Figure 3 | Spatiotemporal distribution of generalized water resources during 1999–2018 in Inner Mongolia, China.

scarce precipitation and few rivers in these regions, therefore, they were the two cities with the lowest AWR in the whole region and faced severe water shortages. The distribution of the cities with high AWR values ($>30 \times 10^8\ m^3$) was located in the northeast of Inner Mongolia, including the cities of HL, TL, XA and CF, the share of the four cities being over 75% of total AWR. Specifically, HL led the region with an AWR level of $177.40 \times 10^8\ m^3$. Compared with the inland northwest region, the cities in the northeast region have obvious advantages in precipitation. At the same time, the rivers in the region are also concentrated in this northeast area, allowing it to have a stronger water storage capacity to obtain rich generalized water resources. For the other six cities covering BT, BY, HH, XL, WL and OR, the value was approximately $16.54 \times 10^8\ m^3$, which is lower than the average of Inner Mongolia. The current situation, with water resources in short supply, may cause ecological and environmental problems.

3.2. CWF

The water footprint (CWF) of the four major crops was calculated as $267.98 \times 10^8\ m^3$ during 1999–2018, of which the WF_{corn}, WF_{beans}, WF_{wheat}, and WF_{tubers} were approximately 150, 48, 31 and $30 \times 10^8\ m^3$, respectively. The CWF of each crop is shown in Figure 4. The CWF was maintained at $196.41 \times 10^8\ m^3$ from 1999 to 2003 and then gradually this was followed by an increasing trend over time, reaching $353.54 \times 10^8\ m^3$ in 2018. The WF_{corn} soared from $104.29 \times 10^8\ m^3$ to $240.37 \times 10^8\ m^3$ accounting for 58% of the total CWF, while the annual WF_{wheat}, WF_{beans} and WF_{tubers} were approximately $30.16 \times 10^8\ m^3$, $47.44 \times 10^8\ m^3$ and $30.09 \times 10^8\ m^3$, respectively, and none showed noticeable changes during the study period. The primary reason that the CWF increased gradually after 1999 is attributed to the tremendous increase in the WF_{corn}, whose growth rate was 130%. The continuous expansion of arable land and the increase in the use of fertilizer led to the growth in WF_{corn}. During the observed period, the arable land for corn expanded from 1.57×10^6 ha to 3.72×10^6 ha, and the ground fertilizer used in 2018 was greater by 78% than in 1999 while the effective utilization rate did not improve (Fan *et al.* 2012). In addition, the precipitation increased from 223.2 mm to 328.2 mm, and although the annual precipitation varied greatly, it had little effect on P_{eff}. Since P_{eff} does not increase linearly with precipitation (Xinchun *et al.* 2017b), it has only a slight effect on WF_{corn}. All the above reasons promoted the increase in WF_{corn}, yielding the variation in the annual CWF.

From the perspective of spatial distribution, the CWF values are mainly determined by the scale of agricultural production in cities, so the CWF of different cities varies greatly. The regional CWF ranged from $59.02 \times 10^8\ m^3$ to $0.54 \times 10^8\ m^3$. The spatial distribution pattern of the CWF in cities in Inner Mongolia from 1999 to 2018 is shown in Figure 5.

During the study period, the CWF exhibited considerable spatial aggregation, with a gradual decrease from northeast to southwest (Figure 5). The four cities in the northeast maintained high CWF, followed by those in the central region. The CWF values are lower in the southwest region and in XL. The lowest CWF was found in WH and was only $0.54 \times 10^8\ m^3$. The CWF of AL and XL were $1.38 \times 10^8\ m^3$ and $4.00 \times 10^8\ m^3$, respectively, which is considered low in Inner Mongolia. The CWF of the other four cities, namely, BT, OR, HH, and WL, did not exceed the average value of $21.54 \times 10^8\ m^3$ in the region. The CWF of the remaining five cities of HL, TL, XA and CF in the northeast region and BY in the west region were higher than the average value, ranging from $22.40 \times 10^8\ m^3$ in BY to $58.02 \times 10^8\ m^3$ in TL. The high values found in HL, TL, XA and CF were caused by the crop planting areas and precipitation. HL has the largest planting area, which is approximately 1.15×10^6 ha, the planting area of the above four cities accounting for 67% of the total planting area of the

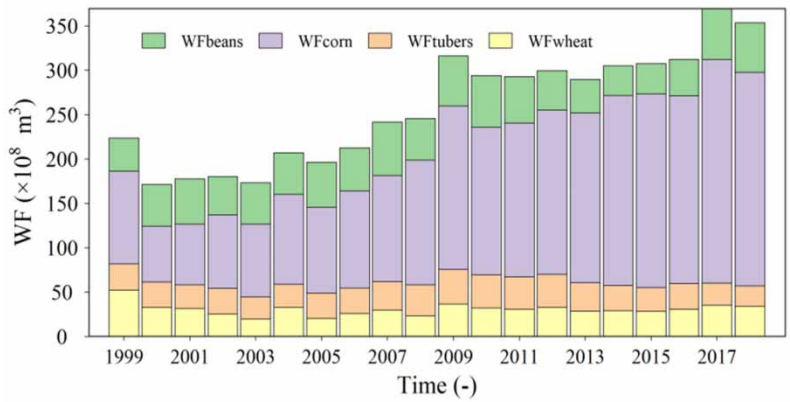

Figure 4 | Water footprints of different crops in Inner Mongolia during 1999–2018.

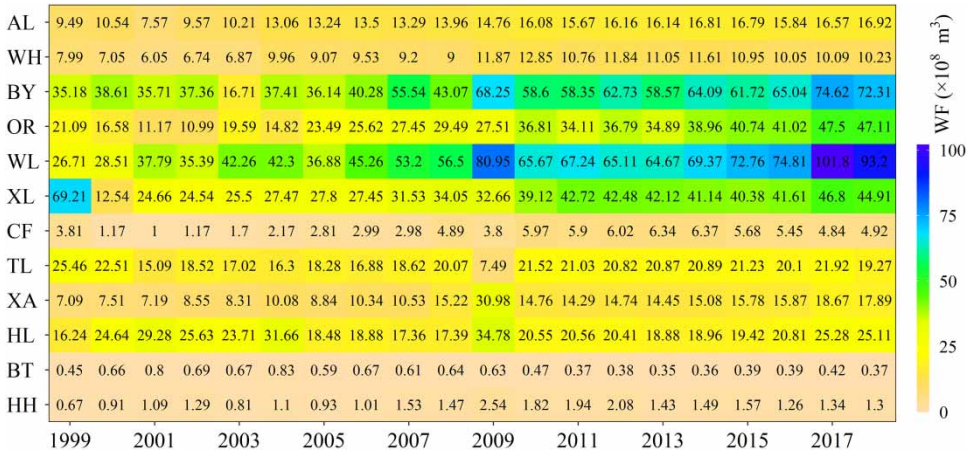

Figure 5 | The total amounts of the crop water footprints of 12 cities in Inner Mongolia during 1999–2018.

four crops in Inner Mongolia. The planted area had positive effects on the blue, green and grey water footprints (Cao *et al.* 2018). Simultaneously, the area received the most rainfall, and effective rainfall had a positive impact on the blue and green water footprints. Additionally, the CWF of BY was higher than the average, primarily resulting from the largest irrigation scale, with an effective irrigation area of 6.06×10^6 ha, a share of 25.6% of the total, which promoted the CWF of the city (Darré *et al.* 2019). In contrast, the lowest CWF in WH and AL is attributed to agricultural scale and precipitation, because WH has the smallest urban area, at only 0.18×10^6 ha. In addition, it is an industrial city with a small agricultural scale; thus, the CWF in this city is the smallest. AL is located in the hinterland of Eurasia, so there is little precipitation and high evaporation. Mountains, hills, and desert areas (such as the Gobi Desert) in this area account for 84% of the total area. The harsh natural conditions are not suitable for the development of agriculture, resulting in a small CWF.

3.3. AWSI

From 1999 to 2018, the annual generalized water resources (AWR) and crop water footprint (CWF) of Inner Mongolia were 419.64×10^8 m^3; and 258.52×10^8 m^3, respectively. Therefore, the annual AWSI was approximately 0.63 during the study period. This suggests that the cultivated land in Inner Mongolia is generally under high water stress and serious water shortage. The annual AWR, CWF and AWSI were calculated during 1999–2018, and the yearly values and the corresponding trend lines during the period are shown in Figure 6 to identify the variation of AWSI over time in Inner Mongolia. Figure 6 shows that the AWR in Inner Mongolia fluctuates significantly from year to year, however, it climbs slowly over time. The maximum AWR value was 651.80×10^8 m^3 in 2013, and the minimum value was 285.70×10^8 m^3 in 2000. This is mainly attributed to the stability of overall climate, total water consumption and water structure. Generally, the CWF increased from

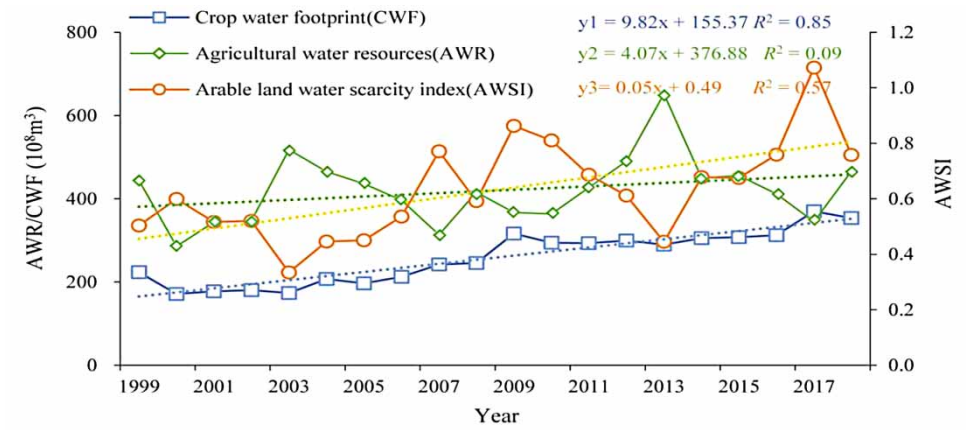

Figure 6 | Changes in CWF, AWR and AWSI over time in Inner Mongolia during 1999–2018.

171.24×10^8 m^3 to 369.84×10^8 m^3. The expansion of the area of arable land and adjustments to crop planting methods are the fundamental reasons for the continued growth of the CWF. The AWSI ($p < 0.001$) is determined by the sizes and fluctuations of the AWR and CWF. The average annual growth rates of the AWR and CWF were 0.25% and 0.75%, respectively. Although both terms increased over the study period, the average annual growth rate of the CWF was greater, so the AWSI shows a rising trend. From 1999 to 2006, the AWSI was lower than the regional average, stabilized at 0.49, and fluctuated slightly, denoting high water stress. In this time period, the AWSI in 2003 was 0.33, indicating moderate water stress. After 2007, the average AWSI was 0.73, and the fluctuation range climbed. In 2009, 2010 and 2017, the AWSI was 0.86, 0.81 and 1.07, respectively, facing very high water stress. Moreover, the peak value of 1.07 in 2017 exceeds 1, suggesting that the actual agricultural water consumption in Inner Mongolia in 2017 exceeded the available generalized water resources, revealing that grey water pollution is very serious (Chukalla *et al.* 2018). Inner Mongolia is facing a severe water shortage test, and the uncertainty is increasing.

The Moran's *I* values of Inner Mongolia's arable land water scarcity index are shown in Figure 7. Except for 2007, 2012 and 2013, all other years had values of approximately 0, and the corresponding *Z*-scores were less than the threshold of 1.65, with a credibility of 90% (Figure 7). Although the *Z*-scores in 2007, 2012 and 2013 were greater than 1.65, the Moran's *I* values were still close to 0, indicating that Inner Mongolia's AWSI showed complete spatial randomness, and the AWSI of each city was spatially random. The AWSI is affected by complex factors such as climatic conditions, water use structure, and social and economic conditions (Chen *et al.* 2020), and the above elements show that the randomness of these factors in the cities may be the key to the spatial random distribution of the AWSI of the cities.

To analyse the spatial characteristics of the AWSI more deeply, the spatial distribution map of AWSI in 1999 and 2018 and the rate of change of each city during the study period is given in Figure 8. The AWSI changed differently over time among the cities in Inner Mongolia, and the overall trend was of increasing water stress. The AWSI of BT, CF, WL, BY and WH were all higher than 0.8, and the rates of change in these cities were less than 2%, thus they were under very high water stress and remained unchanged. Fortunately, the AWSI in WH and BY showed negative growth; specifically, the growth rate of WH was as low as −17.3%, which eased the pressure on water resources. The rates of change in XL and XA were 1.2% and 1.6% and the degrees of water shortage for arable land were revealed to be moderate at 0.22 and high at 0.66, respectively. The other five cities of HH, TL, OR, HL, and AL had higher rates of change. HH and TL changed from high water stress in 1999 to very high water stress in 2018; HL and OR changed from low water stress and moderate water stress, respectively, to high water stress, and AL changed from 0.06 (no water stress) in 1999 to 1.20 (very high water stress) in 2018. The rising pressure on water resources poses a serious threat to agricultural production. These regions urgently need to take effective actions to alleviate water shortages, such as adjusting the agricultural industry and reducing the proportion of high-water-demand cereal crops (Wu *et al.* 2019).

The annual average value, median, range, standard deviation, and average annual growth rate of the AWSI in the cities were also calculated and are shown in Figure 9. In general, the spatial form of the AWSI in Inner Mongolia is consistent with Moran's *I*. During 1999–2018, XL and HL, the areas with the smallest AWSI, were under moderate water stress, followed by XA and OR, which were facing high water stress; the remaining cities were facing very high water stress. During the study period, the annual average AWSI was 0.22 in XL, showing moderate water stress ($0.20 < \text{AWSI} < 0.40$), this

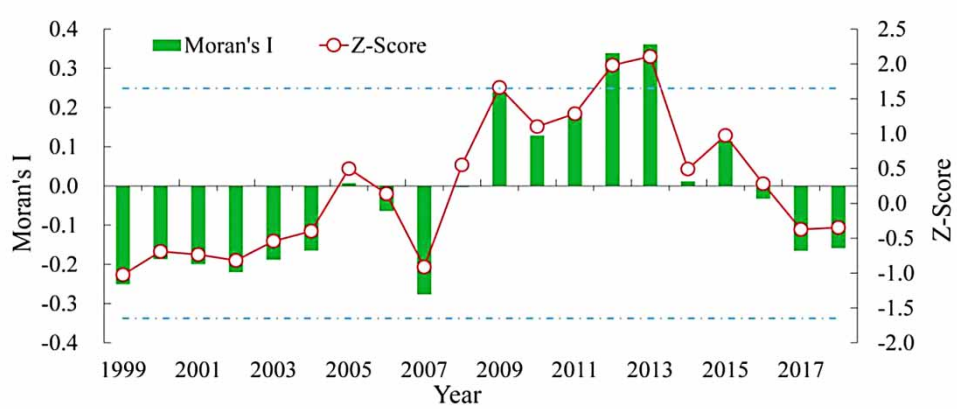

Figure 7 | Global Moran's *I* (and its test) of the AWSI of Inner Mongolia during 1999–2018 (dotted line *Z*-score = ±1.65).

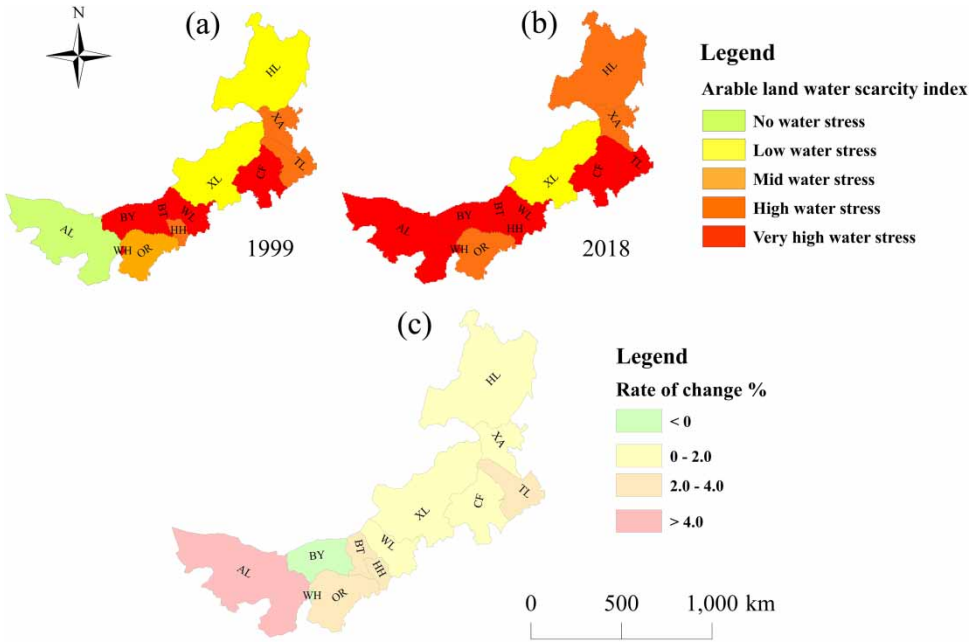

Figure 8 | Spatial distribution of the AWSI in (a) 1999 and (b) 2018 (b), and (c) the change rate of the AWSI during 1999–2018.

being the city with the fewest challenges to arable land and water resources in Inner Mongolia, which significantly stems from the planting area. The AWR in XL was at the middle level of the entire region and annual average AWR was close to $18.98 \times 10^8\ m^3$. Although the water supply conditions are not ideal, the main industry in XL is animal husbandry, so the scale of agricultural production is small; it is the third-smallest city behind WH and AL in planting area. In XL, the planting area of the four main crops was approximately 0.09×10^6 ha. The annual average CWF was $4.00 \times 10^8\ m^3$, so the ratio of CWF and AWR caused the smallest AWSI. Next, the AWSI value of HL was 0.32, which belonged to the medium water stress category. Because the agricultural production scale in HL was the highest in the entire region, and the area of the four main crops was approximately 1.15×10^6 ha. The scale of agricultural production is large in this city, and the total water footprint of crops is also large. The annual average CWF was $51.01 \times 10^8\ m^3$. The available water resources are abundant, and the average annual agricultural available water resources in the observation year were close to $177.40 \times 10^8\ m^3$; these reasons led to low AWSI in HL. The cities of OR and XA were under high water stress ($0.40 < \text{AWSI} < 0.80$), and the AWSI values of the remaining eight cities soared from 0.83 in HH to 3.18 in WH. The AWSI values obviously exceeded the high water stress threshold of 0.80, showing that these areas are facing very high water stress. WH has the most seriously shortage in water, which is attributed to it having the smallest area in the region, so its water resources and arable land area are relatively small, at $0.18 \times 10^8\ m^3$ and 0.01×10^6 ha, respectively. In WH, the green, blue and grey water footprints were $0.05 \times 10^8\ m^3$, $0.13 \times 10^8\ m^3$ and $0.35 \times 10^8\ m^3$. The grey water footprint accounted for 65% of the CWF, thus, grey water pollution has severely impacted the agricultural water use process.

The median, range, standard deviation, and average annual growth rate of the AWSI were also calculated and are shown in Figure 9. The annual average and median values of the AWSI in each city were slightly different, but except for in WH, the overall trend of the two was highly consistent. The annual average and median of the AWSI in WH are 3.18 and 2.80, respectively. The abnormal difference between the two is because the general precipitation of WH from 2000 to 2002 was small, resulting in a large average AWSI. The range and standard deviation had a highly consistent spatial distribution with the AWSI. The higher the AWSI value of a city, the greater the range of inter-annual variation, and the lower the stability. For example, the ranges in WH, BY and AL were greater than 2.00. In contrast, the range and standard deviation in XL and HL were relatively low. In particular, the range in XL was approximately 0.34, and the standard deviation was 0.10. The range, standard deviation, and average values indicate that XL and HL face less water stress than the other cities. On the other hand, these values show that the water stress in these two cities has remained stable over time. The standard deviations in the other ten cities were between 0.18 (WL) and 1.21 (WH), which is quite a large range. WH and BY had the largest AWSI, but the average annual growth rates of the AWSI in these regions were negative, suggesting that the shortage of arable land in these two cities improved.

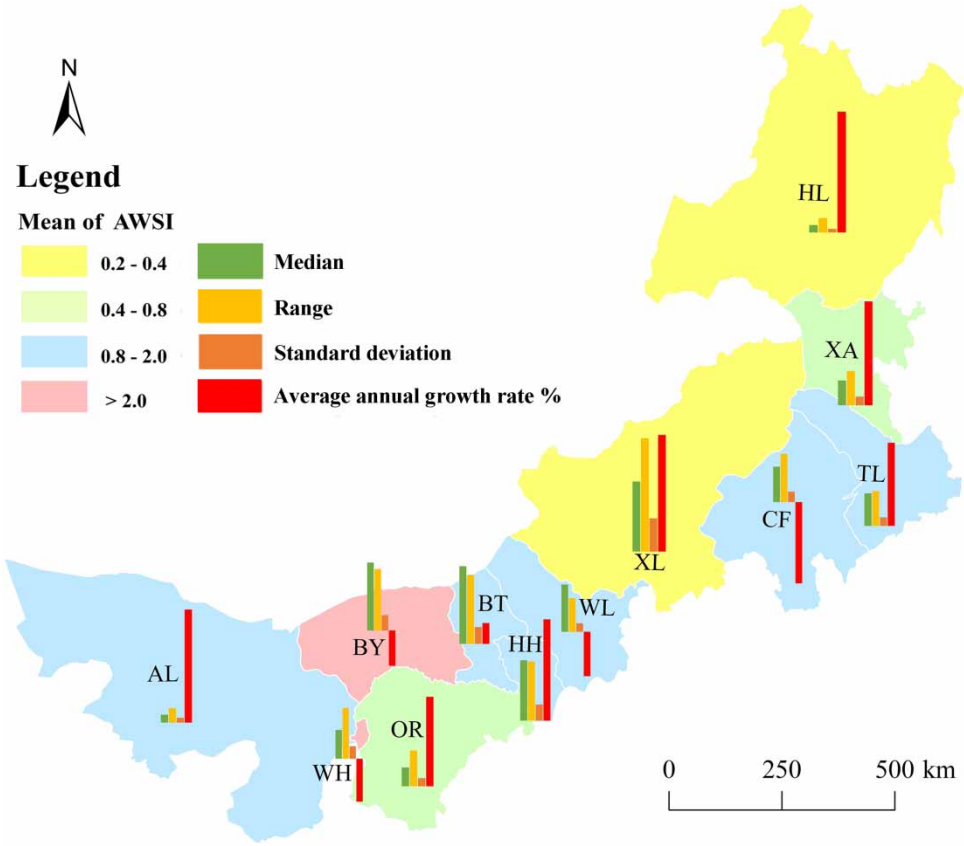

Figure 9 | Mean and other major statistics of the AWSI of Inner Mongolia during 1999–2018 (histogram shows the major statistics).

The average annual growth rate of AL reached 16.5%, which was significantly higher than that in the other cities. The AWR in AL decreased from 11.87×10^8 m^3; in 1999 to 3.38×10^8 m^3 in 2018, while the CWF was boosted from 0.67×10^8 m^3 to 1.38×10^8 m^3 in 2018. Excessive fluctuations in the agricultural water resource gap have transformed AL from an area experiencing a short-term water shortage to a medium-level water stress zone to a very high water stress zone. The average annual growth rates of the AWSI in the remaining cities were less than 6%. The inflow and outflow of water resources and the planting area of crops are the direct reasons for the local distribution of AWSI. In addition, using fertilizer excessively is the cause of the most unsustainable use of cultivated land water resources (Zhang *et al.* 2018). The geographical differences in these conditions formed the spatial pattern seen, that is, the random distribution of the AWSI in Inner Mongolia.

3.4. Driving factors of AWSI

The spatiotemporal distributions of and changes in AWSI are affected by many factors, including natural and man-made activities. The first potential factor selected by the partial least-squares regression (PLSR) model, t1, can explain 74% of the information of the dependent variable ASWI. The two latent factors t1 and t2 can explain 83% of the information of the dependent variable. However, adding more latent factors to the PLSR model of AWSI cannot improve the explanatory value. The weights of t1 and t2 of the PLSR component of AWSI in the whole of Inner Mongolia are shown in Figure 10, which indicates that the planting area proportion (GA) of the four crops in the total crop area accounted for a large proportion in both t1 and t2 and had a positive effect on the potential factors. The larger the planting area proportion, the greater the agricultural water consumption (Singh 2018). The precipitation (P) and relative humidity (RH) inhibit t1. The precipitation and relative humidity in the eastern part of Inner Mongolia are relatively large, and AWSI is generally small. Regarding the latent factor t2, GDP per capita (GP) had a positive impact, while temperature (AT) had a negative impact. Land-average mechanical power (MP) and wind speed (WS) have little effect on the temporal and spatial distribution and changes of regional AWSI.

A factor that has a parametric variable projection importance index (VIP) greater than 1 is more effective in revealing the dependent variable AWSI than is a factor with a VIP less than 1. The PLSR model based on the AWSI in the whole of Inner

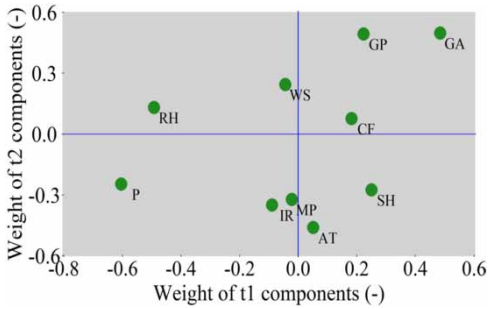

Figure 10 | Weight of t1 and t2 PLSR components for AWSI.

Mongolia (Figure 11) shows that the independent variables with VIP values exceeding 1 are the proportion of the planting area of the four main crops to the total crop (GA; VIP = 1.54, RC = 1.383), precipitation (P; VIP = 1.91, RC = −0.002) and relative humidity (RH; VIP = 1.56, RC = −0.032). The abovementioned planting area proportion (GA) has a regression coefficient of 1.383 and is significantly positively correlated with the AWSI, while precipitation (P) and relative humidity (RH) are negatively correlated with the AWSI. In addition, the factors with relatively small VIP include wind speed (WS; VIP = 0.31) and land-average mechanical power (MP; VIP = 0.39).

Because of the meteorological factors in Inner Mongolia, precipitation generally shows a pattern of decreasing gradually from northeast to southwest and is directly related to the CWF and AWR. Arable land can use the green water directly supplied by precipitation, and precipitation is inseparable from the total amount of water resources in the area, which in turn affects the blue water used for irrigation. The relative humidity distribution is similar to that of the precipitation, as increased precipitation causes increased air humidity, and reduced water vapor evaporation is beneficial to the maintenance of soil moisture (Tomita *et al.* 2018), so both precipitation and relative humidity play a role in hindering the growth of the AWSI. The GA values of the socio-economic factors show the support level of Inner Mongolia's economic foundation and the social conditions for agricultural production. Wheat, corn, beans and tubers are all high water-consumption crops, and the total water footprint of crops tends to be larger in cities with larger planting areas, which in turn leads to increased AWSI values. The difference in MP among the cities was not as obvious as the differences in the other socioeconomic factors, and MP had no effect on the grey water footprint or the generalized water resources, so the impact on the lack of total agricultural water resources was small. In addition, irrigation rate (IR) is a potential factor that significantly affects the AWSI; its regression coefficient (RC) was −0.783, and the AWSI decreased as the IR increased. However, because IR does not change substantially (it was 0.35 in 1999, reached a maximum value of 0.48 during the study period in 2009, and returned to 0.39 in 2018), it has very little impact on the actual changes in AWSI, which is also the reason why the VIP value of IR is low.

The stronger the ability is of an independent variable to explain underlying factors, the more the information it contributes to the AWSI. Table 2 shows the influencing factors of the AWSI in each city and indicates that each city is significantly affected by multiple factors at the same time. The three variables that mainly affect the AWSI all play positive roles: per

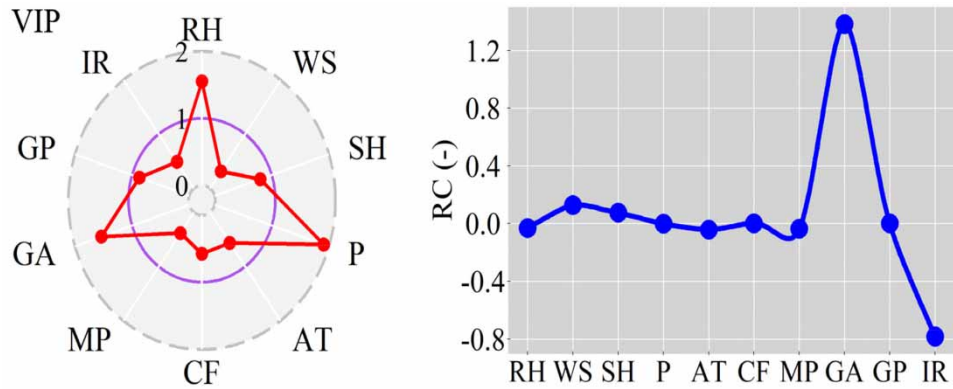

Figure 11 | Variable importance for the projection (VIP, left) and regression coefficients (RC, right) for each predictor of AWSI.

Table 2 | Variable importance of the projection (VIP) for each city of the AWSI

	RH	WS	SH	P	AT	CF	MP	IR	GA	GP
HH	1.49	0.74	0.17	1.71	0.52	1.03	1.13	0.65	0.56	1.07
BT	1.05	0.58	0.08	1.36	0.61	1.20	1.36	0.51	1.22	1.14
HL	1.02	0.82	0.50	0.88	0.05	1.13	1.04	1.05	1.44	1.23
XA	1.55	0.15	0.44	0.82	0.70	1.63	1.04	0.32	0.31	1.57
TL	0.77	1.04	0.32	0.61	0.55	1.31	1.20	1.19	1.25	1.05
CF	0.54	0.92	0.75	0.40	0.51	1.95	1.02	0.56	1.25	1.09
XL	0.58	0.46	0.72	0.78	0.06	0.85	1.08	1.37	1.74	1.17
WL	1.45	0.30	0.72	2.28	0.80	0.68	0.42	0.20	0.81	0.54
OR	0.97	0.58	0.35	1.09	0.04	1.81	1.25	0.94	0.91	0.99
BY	1.05	0.17	1.20	2.35	0.31	0.26	0.56	0.47	0.89	0.67
WH	0.59	0.93	0.79	1.06	0.69	0.86	0.87	0.76	1.44	1.57
AL	1.08	0.65	0.62	0.35	0.63	1.55	0.61	0.70	0.32	2.01

capita gross national product (GP), land-average fertilizer (CF) and land-average mechanical power (MP). In contrast, wind speed (WS), sunshine (SH), average temperature (AT) and irrigation rate (IR) have little effect on the AWSI of each city. The AWSI increases with increasing GP. The GDP per capita measures the level of economic development and affects the water shortage of cultivated land through the water use structure of various industries. In cities with high GPS, the high level of economic development in the secondary and tertiary sectors leads to a high consumption of water resources, while the small proportion of water allocated to the agricultural sector leads to an increase in AWSI (Fan *et al.* 2018). The MP factor includes machinery involved in the agricultural production process, from sowing and irrigation to the final harvest. MP reflects the needs of the planting area and of irrigation. After a planting area is expanded, the water demand of the crops increases, and when rainfall cannot meet the needs of crop growth, farmland irrigation plays a supplementary role. Therefore, after the increase in MP, the shortage of farmland water continues to increase. The impact of CF on AWSI is reflected in the fact that the problem of low fertilizer utilization has not been resolved (Zhang *et al.* 2015; Yang & Lin 2019). The rest of the fertilizer infiltrates into the ground via rainwater, forming polluted grey water that cannot be recycled. On the one hand, the increase in grey water leads to an increase in the water footprint; on the other hand, it leads to a decrease in generalized water resources, both of which contribute to the increase in AWSI. Higher relative humidity (RH) is beneficial for preventing water loss from cultivated land and therefore reduces the AWSI (Qi *et al.* 2018). The proportion of the planting area of the four main crops to the total crop area (GA) has a positive effect on the AWSI. Table 2 also shows that cities in the east with abundant rainwater and sufficient water storage capacities, such as HL, XA, TL, and CF, are less affected by rainfall. In contrast, water shortages in cities in the central and western regions, such as BY, WL, and HH, are severely affected by rainfall. The AWSI of each city is the result of multiple factors, but each factor has a different degree of influence on each of the different cities.

4. CONCLUSIONS

The current study used the CROPWAT model to calculate the blue water, green water and grey water footprints of wheat, corn, beans and tubers and then obtained the total water footprint (CWF) of the major crops in the study region over the past 20 years. Water resource data was used to calculate generalized water resources (AWR). Both the CWF and AWR were used for the arable land water scarcity index (AWSI). Then, the spatiotemporal distributions and the influencing factors of the AWSI in the observed period were explored with the help of spatial autocorrelation analysis. Considering the above, the following conclusions are drawn:

(1) The AWSI realizes the quantitative calculation of available water resources in the region. Inner Mongolia's AWSI ranges from 0.5 in 1999 to 0.76 in 2018, and the average value during the study period is 0.63. Thus, Inner Mongolia is in a state of high water stress and shows an upward trend over time. The water shortage problem, caused by the two human factors of low water resource utilization efficiency and agricultural water pollution, urgently needs to be solved.

(2) The spatial scale of the arable water scarcity index is random. The cities of WH and BY face the most severe stress challenges of arable water resources. Fortunately, the increase rate in the shortage of farmland water has slowed. The cities of XL and HL have the smallest farmland water shortages. However, water shortages in the cities continue to worsen.
(3) The AWSI in Inner Mongolia has close relationships with precipitation, relative humidity, and the proportion of major crops. Every city in Inner Mongolia is significantly impacted by GDP, land-average mechanical power, and land-average fertilizer. Improving the utilization rate of chemical fertilizers, adjusting the planting structure of crops, and controlling crop water consumption while ensuring the output of agricultural products will achieve the sustainable use of water resources, thereby alleviating water stress.

In view of the shortage of agricultural water resources in Inner Mongolia, corresponding measures for the rational utilization of agricultural water resources must be proposed in order to realize the sustainable utilization of water resources as follows: (i) improving the efficiency of surface water utilization and controlling the exploitation of groundwater, (ii) optimizing agricultural planting structure and strengthening the construction of the agricultural water resources management system, (iii) developing and promoting biological water conservation techniques vigorously, (iv) deploying the main grain-producing areas scientifically. Generally, this study will provide vital information for developing appropriate strategies for the rational utilization of water resources and sustainable development of Inner Mongolia.

ACKNOWLEDGEMENTS

We acknowledge funding of the Natural Science Foundation of Inner Mongolia (2020BS03042 and 2020BS04009), Research Start-up Fund Project for Introducing Talents (5909001803 and 1004031904), and National Natural Science Foundation of China (42101030).

DECLARATION OF INTEREST STATEMENT

The authors declare no conflicts of interest.

DATA AVAILABILITY STATEMENT

All relevant data are available from an online repository or repositories (see section 2.2).

REFERENCES

Cao, X., Ren, J., Wu, M., Guo, X. & Wang, W. 2018 Assessing agricultural water use effect of China based on water footprint framework. *Transactions of the Chinese Society of Agricultural Engineering* **34** (5), 1–8.

Castellanos, M. T., Cartagena, M. C., Requejo, M. I., Arce, A., Cabello, M. J., Ribas, F. & Tarquis, A. M. 2016 Agronomic concepts in water footprint assessment: a case of study in a fertirrigated melon crop under semiarid conditions. *Agricultural Water Management* **170**, 81–90.

Chen, M., Luo, Y., Shen, Y., Han, Z. & Cui, Y. 2020 Driving force analysis of irrigation water consumption using principal component regression analysis. *Agricultural Water Management* **234**, 106089.

Chukalla, A. D., Krol, M. S. & Hoekstra, A. Y. 2018 Trade-off between blue and grey water footprint of crop production at different nitrogen application rates under various field management practices. *Science of The Total Environment* **626**, 962–970.

Dai, M., Huang, S., Huang, Q., Leng, G., Guo, Y., Wang, L., Fang, W., Li, P. & Zheng, X. 2020 Assessing agricultural drought risk and its dynamic evolution characteristics. *Agricultural Water Management* **231**, 106003.

Darré, E., Cadenazzi, M., Mazzilli, S. R., Rosas, J. F. & Picasso, V. D. 2019 Environmental impacts on water resources from summer crops in rainfed and irrigated systems. *Journal of Environmental Management* **232**, 514–522.

Egan, M. 2011 The water footprint assessment manual. Setting the global standard. *Social and Environmental Accountability Journal* **31** (2), 181–182.

Falkenmark, M., Lundqvist, J. & Widstrand, C. 1989 Macro-scale water scarcity requires micro-scale approaches: aspects of vulnerability in semi-arid development. *Natural Resources Forum* **13** (4), 258–267.

Fan, M., Shen, J., Yuan, L., Jiang, R., Chen, X., Davies, W. J. & Zhang, F. 2012 Improving crop productivity and resource use efficiency to ensure food security and environmental quality in China. *Journal of Experimental Botany* **63** (1), 13–24.

Fan, J., Wang, J., Zhang, X., Kong, L. & Song, Q. 2018 Exploring the changes and driving forces of water footprints in China from 2002 to 2012: a perspective of final demand. *Science of The Total Environment* **650**, 1101–1111.

Gosling, S. N. & Arnell, N. W. 2016 A global assessment of the impact of climate change on water scarcity. *Climatic Change* **134** (3), 371–385.

Huang, J., Yu, H., Guan, X., Wang, G. & Guo, R. 2016 Accelerated dryland expansion under climate change. *Nature Climate Change* **6** (2), 166–171.

Huang, J., Zhang, G., Zhang, Y., Guan, X., Wei, Y. & Guo, R. 2020 Global desertification vulnerability to climate change and human activities. *Land Degradation & Development* **31** (11), 1380–1391.

Lesk, C., Rowhani, P. & Ramankutty, N. 2016 Influence of extreme weather disasters on global crop production. *Nature* **529** (7584), 84–87.

Li, C., Xiong, Y., Qu, Z., Xu, X., Huang, Q. & Huang, G. 2018 Impact of biochar addition on soil properties and water-fertilizer productivity of tomato in semi-arid region of Inner Mongolia, China. *Geoderma* **331**, 100–108.

Liu, J., Wang, Y., Yu, Z., Cao, X., Tian, L., Sun, S. & Wu, P. 2017 A comprehensive analysis of blue water scarcity from the production, consumption, and water transfer perspectives. *Ecological Indicators* **72**, 870–880.

Melandri, G., AbdElgawad, H., Riewe, D., Hageman, J. A., Asard, H., Beemster, G. T. S., Kadam, N., Jagadish, K., Altmann, T., Ruyter-Spira, C. & Bouwmeester, H. 2019 Biomarkers for grain yield stability in rice under drought stress. *Journal of Experimental Botany* **71** (2), 669–683.

Qader, S. H., Dash, J. & Atkinson, P. M. 2018 Forecasting wheat and barley crop production in arid and semi-arid regions using remotely sensed primary productivity and crop phenology: a case study in Iraq. *Science of The Total Environment* **613–614**, 250–262.

Qi, X., Wang, R. Y., Li, J., Zhang, T., Liu, L. & He, Y. 2018 Ensuring food security with lower environmental costs under intensive agricultural land use patterns: a case study from China. *Journal of Environmental Management* **213**, 329–340.

Qian, Y., Dong, H., Geng, Y., Zhong, S., Tian, X., Yu, Y., Chen, Y. & Moss, D. A. 2018 Water footprint characteristic of less developed water-rich regions: case of Yunnan, China. *Water Research* **141**, 208–216.

Raphael, O. D., Ogedengbe, K., Fasinmirin, J. T., Okunade, D., Akande, I. & Gbadamosi, A. 2018 Growth-stage-specific crop coefficient and consumptive use of *Capsicum chinense* using hydraulic weighing lysimeter. *Agricultural Water Management* **203**, 179–185.

Raskin, P., Gleick, P., Kirshen, P., Pontius, G. & Strzepek, K. 1997 *Water Futures: Assessment of Long-Range Patterns and Problems. Comprehensive Assessment of the Freshwater Resources of the World*. Stockholm Environment Institute, Stockholm, Sweden.

Schneider, U. A., Havlík, P., Schmid, E., Valin, H., Mosnier, A., Obersteiner, M., Böttcher, H., Skalský, R., Balkovič, J., Sauer, T. & Fritz, S. 2010 Impacts of population growth, economic development, and technical change on global food production and consumption. *Agricultural Systems* **104** (2), 204–215.

Singh, A. 2018 Assessment of different strategies for managing the water resources problems of irrigated agriculture. *Agricultural Water Management* **208**, 187–192.

Singh Rawat, K., Kumar Singh, S., Bala, A. & Szabó, S. 2019 Estimation of crop evapotranspiration through spatial distributed crop coefficient in a semi-arid environment. *Agricultural Water Management* **213**, 922–933.

Song, J., Yin, Y., Xu, H., Wang, Y., Wu, P. & Sun, S. 2020 Drivers of domestic grain virtual water flow: a study for China. *Agricultural Water Management* **239**, 106175.

Tomita, H., Hihara, T. & Kubota, M. 2018 Improved satellite estimation of near-surface humidity using vertical water vapor profile information. *Geophysical Research Letters* **45** (2), 899–906.

Tripathi, A., Tripathi, D. K., Chauhan, D. K., Kumar, N. & Singh, G. S. 2016 Paradigms of climate change impacts on some major food sources of the world: a review on current knowledge and future prospects. *Agriculture, Ecosystems & Environment* **216**, 356–373.

Wang, Y., Liu, G. & Guo, E. 2018 Spatial distribution and temporal variation of drought in Inner Mongolia during 1901–2014 using Standardized Precipitation Evapotranspiration Index. *Science of The Total Environment* **654**, 850–862.

Wu, D., Fang, S., Li, X., He, D., Zhu, Y., Yang, Z., Xu, J. & Wu, Y. 2019 Spatial–temporal variation in irrigation water requirement for the winter wheat–summer maize rotation system since the 1980s on the North China Plain. *Agricultural Water Management* **214**, 78–86.

Xinchun, C., Mengyang, W., Rui, S., La, Z., Dan, C., Guangcheng, S., Xiangping, G., Weiguang, W. & Shuhai, T. 2017a Water footprint assessment for crop production based on field measurements: a case study of irrigated paddy rice in East China. *Science of The Total Environment* **610–611**, 84–93.

Xinchun, C., Mengyang, W., Xiangping, G., Yalian, Z., Yan, G., Nan, W. & Weiguang, W. 2017b Assessing water scarcity in agricultural production system based on the generalized water resources and water footprint framework. *Science of The Total Environment* **609**, 587–597.

Xu, Z., Chen, X., Wu, S. R., Gong, M., Du, Y., Wang, J., Li, Y. & Liu, J. 2019 Spatial–temporal assessment of water footprint, water scarcity and crop water productivity in a major crop production region. *Journal of Cleaner Production* **224**, 375–383.

Yang, J. & Lin, Y. 2019 Spatiotemporal evolution and driving factors of fertilizer reduction control in Zhejiang Province. *Science of The Total Environment* **660**, 650–659.

Zhai, J., Huang, J., Su, B., Cao, L., Wang, Y., Jiang, T. & Fischer, T. 2017 Intensity–area–duration analysis of droughts in China 1960–2013. *Climate Dynamics* **48** (1–2), 151–168.

Zhang, X., Davidson, E. A., Mauzerall, D. L., Searchinger, T. D., Dumas, P. & Shen, Y. 2015 Managing nitrogen for sustainable development. *Nature* **528** (7580), 51–59.

Zhang, Y., Ma, Q., Liu, D., Sun, L., Ren, X., Ali, S., Zhang, P. & Jia, Z. 2018 Effects of different fertilizer strategies on soil water utilization and maize yield in the ridge and furrow rainfall harvesting system in semiarid regions of China. *Agricultural Water Management* **208**, 414–421.

Zhang, L., Dong, H., Geng, Y. & Francisco, M.-J. 2019 China's provincial grey water footprint characteristic and driving forces. *Science of The Total Environment* **677**, 427–435.

Zhao, X., Liao, X., Chen, B., Tillotson, M. R., Guo, W. & Li, Y. 2019 Accounting global grey water footprint from both consumption and production perspectives. *Journal of Cleaner Production* **225**, 963–971.

Zhao, C., Gong, J., Wang, H., Wei, S., Song, Q. & Zhou, Y. 2020 Changes of temperature and precipitation extremes in a typical arid and semiarid zone: observations and multi-model ensemble projections. *International Journal of Climatology* **40** (12), 5128–5153.

Zhou, J., Wang, Y., Su, B., Wang, A., Tao, H., Zhai, J., Kundzewicz, Z. W. & Jiang, T. 2020 Choice of potential evapotranspiration formulas influences drought assessment: a case study in China. *Atmospheric Research* **242**, 104979.

First received 3 February 2021; accepted in revised form 4 August 2021. Available online 18 August 2021